

High-risk Factor Prediction in Lung Cancer Using Thin CT Scans: An Attention-Enhanced Graph Convolutional Network Approach

1st Xiaotong Fu

*Center for Applied Statistics
School of Statistics
Renmin University of China
Beijing, China
xiaotongfu@ruc.edu.cn*

2nd Xiangyu Meng

*Center for Applied Statistics
School of Statistics
Renmin University of China
Beijing, China
xiangyumeng@ruc.edu.cn*

3rd Jing Zhou*

*Center for Applied Statistics
School of Statistics
Renmin University of China
Beijing, China
jing.zhou@ruc.edu.cn*

4th Ying Ji*

*Department of Thoracic Surgery
Beijing Institute of Respiratory Medicine
Beijing Chao-Yang Hospital
Capital Medical University
Beijing, China
jiying@mail.ccmu.edu.cn*

Abstract—Lung cancer, particularly in its advanced stages, remains a leading cause of death globally. Though early detection via low-dose computed tomography (CT) is promising, the identification of high-risk factors crucial for surgical mode selection remains a challenge. Addressing this, our study introduces an Attention-Enhanced Graph Convolutional Network (AE-GCN) model to classify whether there are high-risk factors in stage I lung cancer based on the preoperative CT images. This will aid surgeons in determining the optimal surgical method before the operation. Unlike previous studies that relied on 3D patch techniques to represent nodule spatial features, our method employs a GCN model to capture the spatial characteristics of pulmonary nodules. Specifically, we regard each slice of the nodule as a graph vertex, and the inherent spatial relationships between slices form the edges. Then, to enhance the expression of nodule features, we integrated both channel and spatial attention mechanisms with a pre-trained VGG model for adaptive feature extraction from pulmonary nodules. Lastly, the effectiveness of the proposed method is demonstrated using real-world data collected from the hospitals, thereby emphasizing its potential utility in the clinical practice.

Index Terms—Deep Learning, Lung Cancer, Graph Convolutional Network, Attention Mechanism

I. INTRODUCTION

Lung cancer is a leading cause of cancer-related deaths worldwide, posing a significant threat to human health [1]–[3]. In China, for instance, the lack of early symptoms often

This work was supported by the National Natural Science Foundation of China (No.72171226, 62306189) and the National Statistical Science Research Project (No. 2023LD008). *Corresponding authors: jing.zhou@ruc.edu.cn; jiying@mail.ccmu.edu.cn

results in approximately 75% of patients being diagnosed with advanced-stage lung cancer, leading to a considerably low likelihood of cure [4]. The advent of low-dose CT screening has enabled earlier detection of lung cancers, often at stage I, where subpulmonary resection can be as effective as lobectomy while preserving more healthy lung tissue [5]. However, several studies have demonstrated that using the subpulmonary approach for patients with lung cancers who exhibit pathological high-risk factors such as micropapillary, solid, complex glandular, and vascular tumor thrombus, can lead to a higher recurrence rate [6]. Therefore, the accurate identification of stage I lung cancers with pathological high-risk factors is of utmost importance in selecting the appropriate thoracic surgical approach. Currently, surgical decisions are made from intraoperative pathological evaluations. Advancing the determination of an appropriate surgical approach preoperatively, for instance, based on preoperative CT imaging, is a significant yet unmet challenge. Recently, with the rapid development of artificial intelligence (AI), the application of deep learning models in lung CT diagnosis is becoming increasingly widespread. The majority of research focuses on lung nodule segmentation [7], [8], differentiation of benign and malignant nodules [9], [10], and recognition of nodule progression [11]. A latest study by Zhou et al., (2023) have built an online platform, which can not only predict benign and malignant, pre-invasive and invasive nodules, but also can classify the invasive nodules into three different grade risk according to the latest IASLC grading system [12]. However, to the best of our knowledge, there is no research on the identification and classification of the pathological high-risk factors of lung cancer based on preoperative CT images. This

gap likely stems from two major hurdles: the difficulty in accurately annotating pulmonary nodules on CT images with specific pathological high-risk factors, and the challenge in capturing such nodule features, calling for more advanced predictive models.

Motivated to improve thoracic surgical mode selection in stage I lung cancer, we aim to create a new classification method for identifying pathological high-risk factors. Although current lung nodule classification methods have yielded encouraging result, some problems still exist. First, clinically, current methods primarily focus on benign/malignant and pre-invasive/invasive classification, lacking in pathological high-risk factor prediction. Second, technically, they often require 3D patches for model input, making training lengthy and inefficient. Finally, for complex lung lesions like discerning pathological high-risk factors, existing algorithms fall short in managing large data volumes and extracting intricate features. To overcome the aforementioned problems, a graph convolutional network with both channel and spatial attention module is proposed to enhance the extraction of characteristic information from pulmonary nodules and improve the training efficiency. In summary, our contributions are as follows:

- We propose a graph convolutional neural network that integrates an attention-enhanced feature extractor to utilize the spatial information of pulmonary nodules with pathological high-risk factors.
- We develop a novel graph construction method that leverages the nodule's slice-level positional information with GCN, enabling a more effective and less time-consuming model training.
- Compared with the benchmarks models, the proposed method has shown a 9.42% improvement in terms of AUC value.

II. RELATED WORK

In this section, we summarize the related research from two aspects, they are respectively, pulmonary nodule classification and GCN model application.

A. Pulmonary Nodule Classification

Prior studies for the diagnosis of pulmonary nodules mainly relied on radiomic models, which involved extracting thousands of tumor-related features to quantify various image characteristics of lung tumors, including morphological, texture, boundary, and intensity features [13], [14]. Recently, convolutional neural networks (CNNs) have gained increasing attention for their ability to extract features directly from CT images [15], [16]. For instance, Bonavita et al. proposed a 3D CNN model for evaluating nodule malignancy [17]. Furthermore, attention mechanisms, such as the convolutional block attention module (CBAM) [18], have shown promising performance for enhancing deep learning models' accuracy, prompting researchers to explore their application in pulmonary nodule classification. For example, Sun et al.

introduced an attention-embedded complementary-stream convolutional neural network (AECS-CNN) capable of extracting contextual features at different scales [19].

However, most studies focus on classifying benign and malignant or pre-invasive and invasive nodules, scarcely addressing invasive subtype recognition [12]. Notably, no research has tackled pathological high-risk factor classification from preoperative CT images, crucial for surgical planning. This knowledge void drove our proposal of a novel method for predicting pathological high-risk factors in pulmonary nodules.

B. GCN Model Application

The graph convolutional network is an extension of CNN that moves from the Euclidean domain to the graph domain and is extensively used for learning from graph data [20]. With the ability to address modeling challenges associated with non-Euclidean spatial data and extract essential spatial features, GCN has shown promising prospects across different domains. For instance, Yao et al. introduced a unique approach, constructing a comprehensive graph from an entire corpus and employing a GCN model for text classification [21]. Additionally, Choi et al. proposed a GCN-based system that directly estimates the 3D coordinates of human mesh vertices from 2D human pose data [22].

For medical imaging analysis, the significance of GCN lies in its ability to capture and incorporate both local and global interactions among image elements during the learning process. For automated anatomical labeling of coronary arteries, Yang et al. introduced the conditional partial-residual graph convolutional network (CPR-GCN), which takes both position and CT image into consideration [23]. Furthermore, Meng et al. combined CNN and GCN to enhance the accuracy of boundary regression in biomedical image segmentation [24].

Despite GCN's success in various domains, its use in lung nodule classification is limited. For example, Adnan et al. applied GCN for feature extraction in lung cancer subtype classification from whole-slide images (WSIs) [25], but ignored the spatial structure between nodule slices. Recognizing that the sequence order of the nodule slices automatically forms a graph-like structure, we are motivated to leverage GCN to process extracted features for classification task.

III. METHODOLOGY

In this section, we introduce the proposed Attention-Enhanced Graph Convolutional Network (AE-GCN) model for pathological high-risk factor identification in lung cancer. Leveraging attention mechanisms for feature extraction and the GCN for classification, our method is good at adaptively extracting deep features from nodules while capitalizing on their inherent spatial structure. An overview of our method is provided in Fig. 1. Specifically, let c_k^i be the i th slice of a nodule N_k , where k index the nodule number. Then the total input slice of node N_k is denoted as $C_k = \{c_k^1, \dots, c_k^{n_k}\}$, with n_k denoting the total slice number of nodule N_k . Our goal is to build a deep neural network G that predicts Y_k given C_k :

$$P(Y_k = 1|C_k) = G(C_k)$$

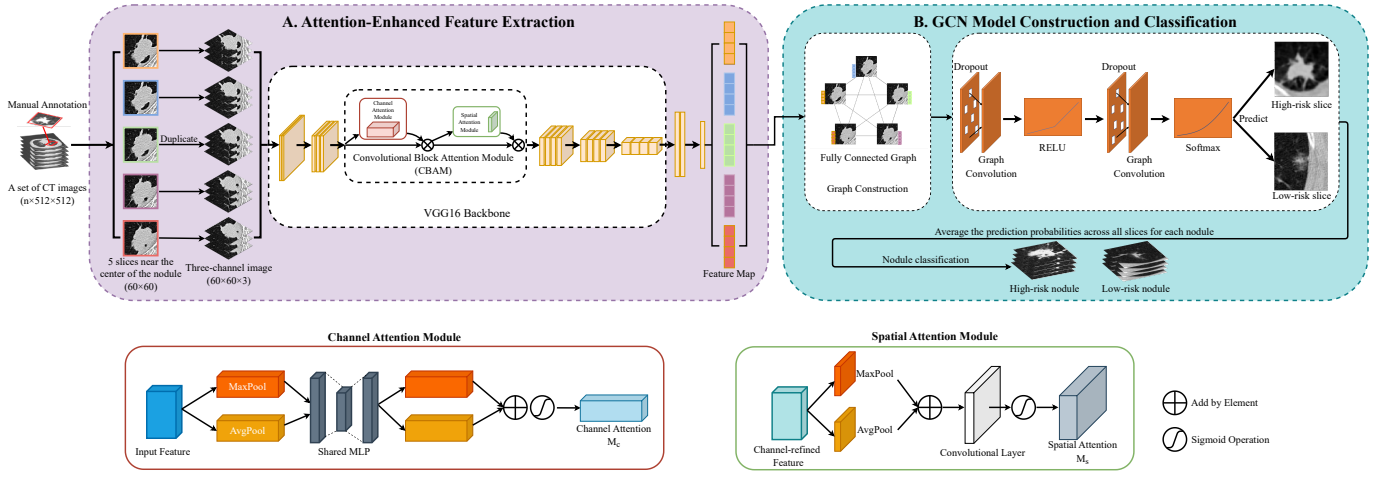


Fig. 1. The structure of the proposed AE-GCN network. Module A represents the CBAM feature extractor, utilizing both channel and spatial attention mechanism on a pre-trained VGG (a zoom-in view of the attention mechanism is provided below). Module B encompasses both the graph construction and GCN classification. The final nodule-level prediction is obtained by averaging the slice-level probabilities.

where $Y_k \in \{0, 1\}$ denotes whether N_k is of pathological high-risk factors.

A. Attention-Enhanced Feature Extraction

For the proposed AE-GCN, a pretrained VGG model is utilized as the backbone for feature extraction. To increase the model performance, we employ a CBAM [18] within the second block of the VGG architecture (See module A in Fig. 1). This module employs both the channel-wise attention, which assesses the significance of different feature channels, and the spatial attention that identifies vital regions within the feature map. This attentional design refines the model by facilitating the extraction of key features, specifically focusing on the Region of Interest (ROI) within lung tissue. Then, we train the attention-enhanced VGG model, denoted by V , on the training set and optimize it on the validation set, thereby tailoring it to effectively extract deep features from pulmonary nodules.

After obtaining V , we can extract the corresponding slice-level feature vector $x_k^i \in \mathbb{R}^{1 \times D}$ for c_k^i as follows:

$$x_k^i = \text{SecondLastLayer}(V(c_k^i)) \quad (1)$$

Subsequently, the nodule-level representation or feature map of the nodule N_k can be defined as $X_k = [x_k^1, \dots, x_k^{n_k}] \in \mathbb{R}^{n_k \times D}$. In our configuration, the feature dimension D is set to be 512.

B. Graph Construction

To construct the graph, we compile the feature maps of all nodules in the training set into a matrix $X = [X_k] \in \mathbb{R}^{N \times D}$, where $N = \sum n_k$ yields the total nodule count. This matrix encapsulates the high-dimensional semantic features of the nodules, with each row corresponding to a specific slice c_k^i of a nodule N_k . We extract x_k^i to represent the attributes of each slice, and the spatial structure of these slices is then used to establish their connectivity.

For each nodule, the information extracted varies with the number of selected slices, n_k . We employ two selection strategies for constructing graph-structured data: a fixed approach and a comprehensive approach. For the fixed strategy, we center around the middle slice and uniformly select two slices on either side, thus, $n_k = 5$. For the comprehensive strategy, we include all CT slices containing the nodule, hence $n_k = \text{SliceNumber}(N_k)$.

For graph construction, we evaluate three distinct methods: star graph, chain graph, and fully connected graph. The distinction among them lies in the different approaches they take to model relationships between slices within a nodule. These varying connective structures facilitate different feature representations, which can significantly influence the effectiveness and performance of the proposed model. For demonstrative purposes, we use $n_k = 5$ as an example and illustrate each method in Fig. 2.

(1) A Star Graph connects each node from the central slice to all other slices, thereby establishing edges between the central node and all others.

(2) A Chain Graph links each node from the bottom slice to the top slice, creating edges only between adjacent slices.

(3) A Fully Connected Graph interconnects all slices within each nodule, constructing edges between any two nodes.

Following the chosen method, we generate the adjacency matrix A , where $A_{ij} = 1$ implies an edge between nodes c_k^i and c_k^j and $A_{ij} = 0$ otherwise. Using the adjacency matrix, we successfully transform CT image data into graph-structured representation data, enabling the extraction of spatial feature information for the GCN model.

C. GCN Classification

After obtaining the feature map X and the adjacency matrix A , we employ the structure of the GCN model proposed by Kipf et al [26] for classification. This model leverages spectral

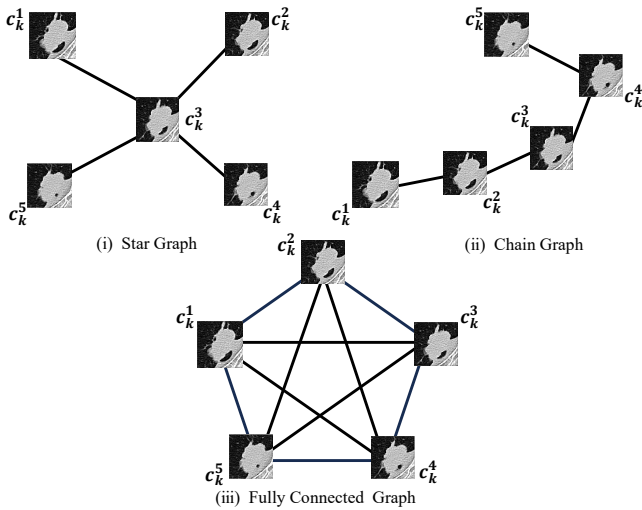


Fig. 2. Illustration of three graph construction methods: star graph, chain graph, and fully connected graph.

graph convolutions and its structure is illustrated as module B in Fig. 1. The specific formula for graph convolution is:

$$H^{(l+1)} = \sigma(\tilde{D}^{-1/2} \tilde{A} \tilde{D}^{-1/2} H^{(l)} W^{(l)}) \quad (2)$$

with $\tilde{D}_{ii} = \sum_j \tilde{A}_{ij}$. In this context, $\tilde{A} = A + I_N$ denotes the adjacency matrix with added self-connections, and I_N is the identity matrix. $\tilde{D}^{-1/2} \tilde{A} \tilde{D}^{-1/2}$ represents the Laplacian matrix of the graph. $W^{(l)}$ is a layer-specific trainable weight matrix, $\sigma(\cdot)$ is an activation function, and $H^{(l)} \in \mathbb{R}^{N \times D}$ is the feature matrix of all nodules in the l th layer, where $H^{(0)} = X$.

The proposed GCN model is composed of two dropout layers and two GCN layers. The first GCN layer, featuring 32 hidden dimensions, uses a Leaky ReLU activation function. Subsequently, the second GCN layer, with two dimensions corresponding to our binary classification task, provides the final probabilistic prediction P obtained by applying a softmax activation function. Defining $\hat{A} = \tilde{D}^{-1/2} \tilde{A} \tilde{D}^{-1/2}$, we can simplify the model as follows:

$$P = H^{(2)} = \text{softmax}(\hat{A} \text{ReLU}(\hat{A} X W^{(0)}) W^{(1)}) \quad (3)$$

Consequently, we have constructed an attention-enhanced GCN model for the identification of high-risk factors in lung cancer, highlighting its potential to detect high-risk pulmonary nodules.

IV. EXPERIMENTS

A. Dataset

The dataset utilized in this study was obtained from two hospitals, including a total of 483 pulmonary nodules collected from 426 patients. Among these nodules, 139 have been identified with pathological high-risk factors, such as micropapillary, solid, complex glandular and vascular tumor thrombus. To ensure an unbiased comparison, we randomly partitioned the patients into three distinct subsets: training, validation, and testing, with an approximate ratio of 6:2:2. The

center coordinates (i.e., X, Y, Z) of each pulmonary nodule were annotated by an experienced thoracic radiologists and their pathological sections were independently reviewed by a professional pathologist to determine whether there are high-risk factors.

The raw CT scans were in Digital Imaging and Communications in Medicine (DICOM) format, with each slice possessing a resolution of 512×512 . In the preprocess procedure, we first converted the DICOM data into Hounsfield Unit (HU) image matrices trimmed to $[-1400, 400]$, which allows our focus on the lung tissues. Subsequently, we normalized the CT values to fall within the range $[0, 1]$ and then centered them around 0 by subtracting the mean value. Finally, the processed images of each nodule were cropped into n_k patches of 60×60 . For data augmentation, we applied various image transformations, such as flipping, rotation, and swapping. Given the single-channel nature of grayscale CT images, we replicated these into a three-channel format, making them suitable for use as input to the proposed CNN feature extractor.

B. Experimental Settings

We fine-tuned the feature extraction module with a starting learning rate of 0.001, reducing it by 50% if no accuracy boost was observed after 20 epochs. The total training was set for 50 epochs using Adam optimizer. For the GCN classification, we set a learning rate of 0.0001, a dropout rate of 0.3, and trained it for 200 epochs. The hyperparameters were set through preliminary experiments to optimize model performance on the validation set. Cross-entropy loss was used for binary classification in both modules. Each model was trained on the training set, and the one with the highest accuracy on the validation set was chosen for further evaluation.

C. Evaluation Metrics

We use various standard metrics such as Area Under the ROC Curve (AUC), accuracy (Acc), sensitivity (Sen), specificity (Spe), positive predictive value (PPV), negative predictive value (NPV), and F1-Score to evaluate model performance. In the GCN classification, slice-level predictions were made. Since a nodule has multiple slices, we averaged the prediction probabilities across all slices per nodule to get a comprehensive nodule-level prediction.

D. Model Variations

To evaluate the AE-GCN model's components, we examined various modifications, focusing on graph construction methods and slice number strategies. First, we probed three graph construction methods: star graph, chain graph, and fully connected graph. Second, we examined data volume impact through two slice number strategies (i.e., n_k): a fixed strategy with $n_k = 5$, and a comprehensive strategy with $n_k = \text{SliceNumber}(N_k)$, including all slices for each nodule.

The evaluation results are summarized in Table I. For model performance evaluation, we used the AUC value as our primary metric and focused on nodular-level metrics. Overall, the fully connected graph outperformed other structures,

TABLE I
PERFORMANCE COMPARISON OF GRAPH CONSTRUCTION METHODS AND PATCH NUMBER IN AE-GCN

Graph Construction	Patch Number	AUC	Acc	Spe	Sen	PPV	NPV	F1
Fully Connected	All	0.9524	0.9355	0.9104	0.8462	0.7857	0.9385	0.8148
Fully Connected	5	0.9432	0.9451	0.9077	0.8846	0.7931	0.9516	0.8364
Chain	All	0.9420	0.9355	0.9552	0.8846	0.8846	0.9552	0.8846
Chain	5	0.9314	0.9011	0.9692	0.7308	0.9048	0.9000	0.8085
Star	All	0.9351	0.9032	0.9403	0.8077	0.8400	0.9265	0.8235
Star	5	0.9207	0.9011	0.8308	0.8077	0.6563	0.9153	0.7241

TABLE II
COMPARISON OF VARIOUS METHODS IN HIGH-RISK FACTOR PREDICTION IN LUNG CANCER

Model	AUC	Acc	Spe	Sen	PPV	NPV	F1
AE-GCN	0.9524	0.9355	0.9104	0.8462	0.7857	0.9385	0.8148
Resnet	0.7738	0.7634	0.8507	0.5385	0.5833	0.8261	0.5600
DenseNet	0.7308	0.6989	0.7164	0.6538	0.4722	0.8421	0.5484
3D Resnet	0.7692	0.7957	0.9104	0.5000	0.6842	0.8243	0.5778
ViT	0.8186	0.7312	0.6716	0.8846	0.5111	0.9375	0.6479
ViT-GCN	0.8582	0.7849	0.8060	0.6923	0.5806	0.8710	0.6316

regardless of the value of n_k . This can be attributed to its capability to better utilize spatial features within the nodules. Furthermore, the comprehensive strategy consistently led to higher AUC values, underlining the benefit of incorporating more information. These results suggest that a more complex graph structure, together with an increased volume of information, can enhance our model’s effectiveness. Consequently, we chose a fully connected graph with a comprehensive strategy as the optimal model for further analysis.

E. Comparison of Different Methods

We compared our proposed model on the testing set against several models that have been extensively studied in previous reports. For end-to-end models, we utilized 2D CNN models such as DenseNet [27] and ResNet18 [28], as well as the recent state-of-the-art Vision Transformer (ViT) [29], and a 3D ResNet18 model [30]. For hybrid models, we also evaluated a GCN model with ViT serving as the feature extractor (ViT-GCN). This was done to validate the effectiveness of the attention mechanism in comparison to the transformer structure for leveraging contextual information in feature extraction. The results of these comparisons are presented in Table II. As we can see, the proposed model outperformed others across most metrics by a considerable margin, with a 9.42% increase for AUC and 13.98% for Acc. This result demonstrated the effectiveness of combining attention-based feature extraction with GCN classification. Specifically, the advantage of the CBAM over the transformer is evident from the superior performance of AE-GCN compared to ViT-GCN. Interestingly, both hybrid models showed comparably higher performance, which can be attributed to the effectiveness of incorporating spatial information via GCN. Meanwhile, context-aware models (i.e., AE-GCN, ViT, and ViT-GCN) consistently surpassed other models in performance, even outperforming 3D Resnet, which is more complex in terms of parameter count. This indicates the importance of employing a more nuanced feature extractor. In addition to performance comparisons, we also conducted a brief analysis of the training

time for the models. The results highlight the efficiency of the proposed AE-GCN model, which takes, on average, less than one second per epoch to complete. In contrast, the traditional 2D CNN model requires over a dozen seconds per epoch, and the 3D CNN model is even more time-consuming, exceeding one minute per epoch. This efficiency in training further underscores the practicality of our approach.

F. Ablation Study

To assess the individual and collective contributions of the channel and spatial attention modules within the CBAM module, we conducted an ablation study using the testing set. This examination scrutinized the impact of including or excluding these attention mechanisms, with the outcomes shown in Table III. The results reveal that both the channel and spatial attention yielded significant improvements in AUC: 11.72% for channel attention, 14.01% for spatial attention, and an even more pronounced 17.92% when combined. These findings underscore the modules’ capability to discern and capture important features, particularly when employed together.

V. CONCLUSION

Identifying high-risk factors in early-stage lung cancers is vital for surgical planning. Currently, surgeons rely on intra-operative pathological analyses for decision-making. However, preoperative determination, such as using CT images, remains a significant challenge. In this paper, we introduce the AE-GCN model, a novel approach combining attentional features with spatial information to tackle this challenge. We develop a novel graph construction method integrating nodule positional information with GCN, enabling more efficient and faster model training. Experimental results demonstrated that the proposed model outperforms many of the previous benchmarks, yielding an increase of 9.42% in AUC value. The AE-GCN model enables thoracic surgeons to assess the high-risk probability of pulmonary nodules using only CT images, aiding in preoperative surgical planning.

TABLE III
ABLATION STUDY ON ATTENTION MECHANISMS

Channel Attention	Spatial Attention	AUC	Acc	Spe	Sen	PPV	NPV	F1
Yes	Yes	0.9524	0.9355	0.9104	0.8462	0.7857	0.9385	0.8148
Yes	No	0.8123	0.7742	0.7910	0.6923	0.5625	0.8689	0.6207
No	Yes	0.8352	0.7742	0.8209	0.6923	0.6000	0.8730	0.6429
No	No	0.7732	0.7634	0.7910	0.6923	0.5625	0.8689	0.6207

REFERENCES

- [1] H. Sung, J. Ferlay, R. L. Siegel, M. Laversanne, I. Soerjomataram, A. Jemal, and F. Bray, "Global cancer statistics 2020: Globocan estimates of incidence and mortality worldwide for 36 cancers in 185 countries," *CA-A CANCER JOURNAL FOR CLINICIANS*, vol. 71, no. 3, pp. 209–249, MAY 2021.
- [2] R. Zheng, S. Zhang, H. Zeng, S. Wang, K. Sun, R. Chen, L. Li, W. Wei, and J. He, "Cancer incidence and mortality in china, 2016," *Journal of the National Cancer Center*, vol. 2, no. 1, pp. 1–9, 2022.
- [3] R. L. Siegel, K. D. Miller, H. E. Fuchs, and A. Jemal, "Cancer statistics, 2022," *CA-A CANCER JOURNAL FOR CLINICIANS*, vol. 72, no. 1, pp. 7–33, JAN 2022.
- [4] "Chinese thoracic, s., [chinese expert consensus on diagnosis of early lung cancer (2023 edition)]," *Zhonghua jie he he hu xi za zhi = Zhonghua jiehe he huxi zazhi = Chinese journal of tuberculosis and respiratory diseases*, vol. 46, no. 1, pp. 1–18, 2023.
- [5] J.-i. Nitadori, A. J. Bograd, K. Kadota, C. S. Sima, N. P. Rizk, E. A. Morales, V. W. Rusch, W. D. Travis, and P. S. Adusumilli, "Impact of micropapillary histologic subtype in selecting limited resection vs lobectomy for lung adenocarcinoma of 2cm or smaller," *JNCI-JOURNAL OF THE NATIONAL CANCER INSTITUTE*, vol. 105, no. 16, pp. 1212–1220, AUG 2013.
- [6] H. Su, H. Xie, C. Dai, S. Zhao, D. Xie, Y. She, Y. Ren, L. Zhang, Z. Fan, D. Chen, F. Jiang, J. Liu, Q. Zhu, J. Yao, H. Ke, C. Wu, G. Jiang, C. Chen, and S. T. A. R. Star, "Procedure-specific prognostic impact of micropapillary subtype may guide resection strategy in small-sized lung adenocarcinomas: a multicenter study," *THERAPEUTIC ADVANCES IN MEDICAL ONCOLOGY*, vol. 12, JUL 2020.
- [7] Y. Xu, L. F. F. Souza, I. C. L. Silva, A. G. Marques, F. H. S. Silva, V. X. Nunes, T. Han, C. Jia, V. H. C. de Albuquerque, and P. P. R. Filho, "A soft computing automatic based in deep learning with use of fine-tuning for pulmonary segmentation in computed tomography images," *APPLIED SOFT COMPUTING*, vol. 112, NOV 2021.
- [8] W. Wu, L. Gao, H. Duan, G. Huang, X. Ye, and S. Nie, "Segmentation of pulmonary nodules in ct images based on 3d-unet combined with three-dimensional conditional random field optimization," *MEDICAL PHYSICS*, vol. 47, no. 9, pp. 4054–4063, SEP 2020.
- [9] H. Wang, H. Zhu, and L. Ding, "Accurate classification of lung nodules on ct images using the transunet," *FRONTIERS IN PUBLIC HEALTH*, vol. 10, DEC 5 2022.
- [10] S. Shen, S. X. Han, D. R. Aberle, A. A. Bui, and W. Hsu, "An interpretable deep hierarchical semantic convolutional neural network for lung nodule malignancy classification," *EXPERT SYSTEMS WITH APPLICATIONS*, vol. 128, pp. 84–95, AUG 15 2019.
- [11] Z.-R. Zhao, Y.-H. Yu, Z.-C. Lin, D.-H. Ma, Y.-B. Lin, J. Hu, Q.-Q. Luo, G.-F. Li, C. Chen, Y.-L. Yang, J.-C. Yang, Y.-B. Lin, and H. Long, "Invasiveness assessment by artificial intelligence against intraoperative frozen section for pulmonary nodules ≥ 3 cm," *JOURNAL OF CANCER RESEARCH AND CLINICAL ONCOLOGY*, Apr 2023.
- [12] J. Zhou, B. Hu, W. Feng, Z. Zhang, X. Fu, H. Shao, H. Wang, L. Jin, S. Ai, and Y. Ji, "An ensemble deep learning model for risk stratification of invasive lung adenocarcinoma using thin-slice ct," *NPJ Digital Medicine*, vol. 6, no. 1, p. 119, 2023.
- [13] L. Wu, C. Gao, P. Xiang, S. Zheng, P. Pang, and M. Xu, "Ct-imaging based analysis of invasive lung adenocarcinoma presenting as ground glass nodules using peri- and intra-nodular radiomic features," *Frontiers in Oncology*, vol. 10, p. 838, 2020.
- [14] X. Hu, W. Ye, Z. Li, C. Chen, S. Cheng, X. Lv, W. Weng, J. Li, Q. Weng, P. Pang *et al.*, "Non-invasive evaluation for benign and malignant subcentimeter pulmonary ground-glass nodules (≤ 1 cm) based on ct texture analysis," *The British Journal of Radiology*, vol. 93, no. 1114, p. 20190762, 2020.
- [15] N. Coudray, P. S. Ocampo, T. Sakellaropoulos, N. Narula, M. Snuderl, D. Fenyö, A. L. Moreira, N. Razavian, and A. Tsirigos, "Classification and mutation prediction from non-small cell lung cancer histopathology images using deep learning," *Nature medicine*, vol. 24, no. 10, pp. 1559–1567, 2018.
- [16] W. Zhao, J. Yang, Y. Sun, C. Li, W. Wu, L. Jin, Z. Yang, B. Ni, P. Gao, P. Wang *et al.*, "3d deep learning from ct scans predicts tumor invasiveness of subcentimeter pulmonary adenocarcinomas," *Cancer research*, vol. 78, no. 24, pp. 6881–6889, 2018.
- [17] I. Bonavita, X. Rafael-Palou, M. Ceresa, G. Piella, V. Ribas, and M. A. Gonzalez Ballester, "Integration of convolutional neural networks for pulmonary nodule malignancy assessment in a lung cancer classification pipeline," *COMPUTER METHODS AND PROGRAMS IN BIOMEDICINE*, vol. 185, MAR 2020.
- [18] S. Woo, J. Park, J.-Y. Lee, and I. S. Kweon, "Cbam: Convolutional block attention module," in *Proceedings of the European conference on computer vision (ECCV)*, 2018, pp. 3–19.
- [19] L. Sun, Z. Wang, H. Pu, G. Yuan, L. Guo, T. Pu, and Z. Peng, "Attention-embedded complementary-stream cnn for false positive reduction in pulmonary nodule detection," *COMPUTERS IN BIOLOGY AND MEDICINE*, vol. 133, JUN 2021.
- [20] D. I. Shuman, S. K. Narang, P. Frossard, A. Ortega, and P. Vandergheynst, "The emerging field of signal processing on graphs: Extending high-dimensional data analysis to networks and other irregular domains," *IEEE signal processing magazine*, vol. 30, no. 3, pp. 83–98, 2013.
- [21] L. Yao, C. Mao, and Y. Luo, "Graph convolutional networks for text classification," in *Proceedings of the AAAI conference on artificial intelligence*, vol. 33, no. 01, 2019, pp. 7370–7377.
- [22] H. Choi, G. Moon, and K. M. Lee, "Pose2mesh: Graph convolutional network for 3d human pose and mesh recovery from a 2d human pose," in *Computer Vision—ECCV 2020: 16th European Conference, Glasgow, UK, August 23–28, 2020, Proceedings, Part VII 16*. Springer, 2020, pp. 769–787.
- [23] H. Yang, X. Zhen, Y. Chi, L. Zhang, and X.-S. Hua, "Cpr-gcn: Conditional partial-residual graph convolutional network in automated anatomical labeling of coronary arteries," in *Proceedings of the IEEE/CVF conference on computer vision and pattern recognition*, 2020, pp. 3803–3811.
- [24] Y. Meng, M. Wei, D. Gao, Y. Zhao, X. Yang, X. Huang, and Y. Zheng, "Cnn-gcn aggregation enabled boundary regression for biomedical image segmentation," in *Medical Image Computing and Computer Assisted Intervention—MICCAI 2020: 23rd International Conference, Lima, Peru, October 4–8, 2020, Proceedings, Part IV 23*. Springer, 2020, pp. 352–362.
- [25] M. Adnan, S. Kalra, and H. R. Tizhoosh, "Representation learning of histopathology images using graph neural networks," *IEEE ACCESS*, 2020.
- [26] T. N. Kipf and M. Welling, "Semi-supervised classification with graph convolutional networks," *CoRR*, vol. abs/1609.02907, 2016.
- [27] G. Huang, Z. Liu, L. Van Der Maaten, and K. Q. Weinberger, "Densely connected convolutional networks," in *Proceedings of the IEEE conference on computer vision and pattern recognition*, 2017, pp. 4700–4708.
- [28] K. He, X. Zhang, S. Ren, and J. Sun, "Deep residual learning for image recognition," *IEEE*, 2016.
- [29] A. Dosovitskiy, L. Beyer, A. Kolesnikov, D. Weissenborn, X. Zhai, T. Unterthiner, M. Dehghani, M. Minderer, G. Heigold, S. Gelly, J. Uszkoreit, and N. Houlsby, "An image is worth 16x16 words: Transformers for image recognition at scale," in *International Conference on Learning Representations*, 2021.
- [30] S. Chen, K. Ma, and Y. Zheng, "Med3d: Transfer learning for 3d medical image analysis," *arXiv preprint arXiv:1904.00625*, 2019.